



Published in final edited form as:

Nanoscale. 2016 December 7; 8(45): 19043–19049. doi:10.1039/c6nr07290a.

Probing Electrical Signals in Retina via Graphene-Integrated Microfluidic Platforms

Yuchen Zhang^{1,+}, Kirsten H. Dodson^{2,+}, Rachel Fischer^{3,4}, Rui Wang⁵, Deyu Li^{2,*}, Rebecca M. Sappington^{3,4,*}, and Ya-Qiong Xu^{1,5,*}

¹Department of Electrical Engineering and Computer Science, Vanderbilt University, Nashville, TN, USA

²Department of Mechanical Engineering, Vanderbilt University, Nashville, TN, USA

³Department of Ophthalmology and Visual Sciences, Vanderbilt Eye Institute, Vanderbilt University Medical Center, Nashville, TN, USA

⁴Department of Pharmacology, Vanderbilt University School of Medicine, Vanderbilt University, Nashville, TN, USA

⁵Department of Physics and Astronomy, Vanderbilt University, Nashville, TN, USA

Abstract

Graphene has attracted extensive attention in biological and biomedical fields due to its unique physical properties and excellent biocompatibility. We combine graphene field-effect transistors and scanning photocurrent microscopy with microfluidic platforms to investigate electrical signals in mouse retina. Remarkable photocurrent signals were detected from the graphene underneath optic nerve head (ONH) of the retina, where the electrical activity from this region can modulate the carrier concentration of the graphene and induce local potential gradients. These built-in electrical potential gradients can efficiently separate photo-excited electron-hole pairs, leading to strong photocurrent responses in the graphene underneath the ONH. We also show that no significant photocurrent signal was observed in the graphene underneath either dehydrated or fixed retinal tissues, verifying that the photocurrent responses generated in the graphene underneath the ONH were indeed induced by the electrical activity in living retina. This method not only provides a way to investigate electrical processes in living retinal tissues, but also offers opportunities to study many other cellular systems involving cell-cell interactions through electrical signaling.

Keywords

graphene; retina; field-effect transistors; scanning photocurrent microscopy; optic nerve head

The retina is a window to the brain and as a part of the central nervous system (CNS), shares similar properties with the brain, making it an ideal candidate for studying physiological and pathological activities in the CNS.^{1–4} Three cellular layers are connected by two layers of

* Author to whom correspondence should be addressed. deyu.li@vanderbilt.edu; rebecca.m.sappington@vanderbilt.edu; yaqiong.xu@vanderbilt.edu.

[†]These authors contributed equally to this work.

synapses formed by the axons and dendrites of neurons in the retina. The outer nuclear layer of the retina contains the cell bodies of light receptors, such as the rods and cones, which are responsible for dim light and precise color vision, respectively. Photoreceptor responses to light stimuli are transmitted as a graded potential through center layers to retinal ganglion cells (RGCs). RGCs, in turn, transmit visual information to the brain via produce action potentials conducted along their axons in the optic nerve. The optic nerve head (ONH) is the region of the retina where RGC axons are bundled together prior to exiting the globe of the eye as the optic nerve proper. This area does not contain neuronal soma and is associated with the “blind spot” in visual perception. However, it is an area of concentrated electrical activity due to the tight bundling of unmyelinated RGC axons.

Various techniques have been developed to study the neural activity in retina and other neural networks. Patch-clamp recording can record voltage or current signals of a single cell with high electrical sensitivity and has been widely used to investigate neural activity *in vitro* and *in vivo*.^{5–8} Nevertheless, the sizeable probe tips and bulky micromanipulators involved in this technique make it challenging to investigate a large population of cells in an entire neural network. Recently, various kinds of fluorescence sensors, such as voltage sensitive dyes and calcium indicators, have been utilized to optically record electrical activities in neural networks with high throughput.^{9, 10} However, the electrical sensitivity of optical imaging is significantly lower than that of patch-clamp recording.¹¹ With high-density electrode arrays, microelectrode arrays (MEAs) can stimulate and record a large population of neurons simultaneously, making it a powerful technique to study the functions and connections of neural networks.^{12–14} Although field effect transistors (FETs) have been applied to improve the electrical sensitivity, electrode density and physical contact problems are still limiting the capability of MEAs in studying neural networks.^{15, 16} The limitations of these currently available neurotechnologies thus call for new approaches to further improve our capability to probe and understand complex neural networks.

After groundbreaking experiments for the micromechanical exfoliation of graphene, it has become one of the most promising candidates for future electronics because of its extraordinary electronical and optical properties.^{17–20} Absorbing merely 2.3% of incident light makes graphene compatible with high-resolution optical imaging. As a two-dimensional material, graphene exposes its whole structure to the environment, making it extremely sensitive to local electrochemical environment changes.²¹ Furthermore, due to its strength, flexibility, and biocompatibility, graphene can attach to cells and tissues to achieve high electrical sensitivity for a long-term experiment, making it an excellent material for biosensing.^{22–24}

Here, we combine graphene FETs with scanning photocurrent microscopy to detect the neural activity of mouse retina, which is placed on microfluidic platforms that can keep whole mouse retina healthy for multiple days.²⁵ Electrical activity in living retinal tissues can modulate the carrier concentration of graphene, resulting in potential gradients that can separate photo-excited electron-hole pairs (EHPs) and produce photocurrent signals. In our experiments, strong photocurrent responses are detected from the graphene underneath ONH, suggesting that the electrical activity of the ONH is sufficient to alter the local electrical properties of graphene. We also find that no remarkable photocurrent response is

detected from the graphene underneath both dehydrated and fixed retina, which further confirm that the photocurrent signals in graphene that we observe are indeed from the electrical activity in living tissues.

RESULTS AND DISCUSSION

Figure 1A shows the components of our graphene-based microfluidic platform: a glass cylinder, a slice of agar gel, a polydimethylsiloxane (PDMS) ring, and graphene transistors. First, graphene was synthesized via a standard chemical vapor deposition (CVD) method and transferred onto 170 μm thick coverslips with pre-patterned gold electrodes.²⁶ We performed Raman spectroscopy measurements to inspect the quality and thickness of graphene on the coverslips with a 532 nm laser. As shown in Figure 1B, the 2D peak has a symmetric shape and the 2D-to-G intensity ratio is about 2, indicating that the as-grown graphene is of a monolayer structure. We also characterized the electrical transport property of graphene transistors. In our experiment, a PDMS ring was placed on top of the chip with graphene transistors and filled with 1X phosphate-buffered saline (PBS) solution. A gold wire was inserted into the cylinder and used as a gate to set the electrochemical potential of the solution. Figure 1C exhibits the ambipolar behavior of a typical graphene transistor with the Dirac point close to 0.7 V, displaying p-type characteristics at zero gate bias.

After fabricating graphene transistors on a thin coverslip, we placed a slice of agar gel at the bottom of a glass cylinder, which serves as a supporting substrate to hold the retina in place as well as a porous pad that allows fresh media to slowly perfuse through to supply nutrients to the retina from the cylinder. Live retina was dissected and mounted on top of the agar gel. The cylinder was then inverted and inserted into the large hole of the PDMS ring, such that the retina came in contact with graphene transistors. Serum-free culture media containing neurotrophic factors was then added to the glass cylinder to maintain the retina health.²⁵ Moreover, the media weight on top of the agar gel helps to hold the cylinder in place on top of the retina to restrict curling. Three days prior to enucleation and retina dissection, mice received an intravitreal injection of fluorophore-conjugated cholera toxin subunit B (CTB). CTB is an active uptake and active transport neural tracer that is preferentially endocytosed by RGCs and anterogradely transported along their axons to the axon terminal in the brain. We utilized the tracer to visualize RGCs and the unmyelinated segment of their axons in the retina and ONH during photocurrent recording.²⁷ As demonstrated in Figure 1D, a CTB-labeled (red) whole retina was placed on top of graphene transistors, where the dark regions are opaque gold electrode arrays. The fluorescence image presents the structure of RGCs layer. All the axons of RGCs from different parts of the retina extend from cell soma, group into bundles, and coalesce at the ONH in the center of the retina to exit the globe of the eye. During our experiments, heating gel pads were used to maintain an external environment of 36 °C. With culture media perfusion through agar gel consistently, the microfluidic platform can sustain whole mouse retina for over 96 hours, as illustrated in our previous report.²⁵

To explore electrical activity in retina, we performed spatially-resolved photocurrent measurements through a graphene-integrated microfluidic platform. A continuous-wave laser source with a wave length of 785 nm was selected to prevent the retina from responding to the laser based on the negligible spectral sensitivity of mouse retina to the

light of wavelength above 700 nm.²⁸ The laser beam was deflected by a nanometer-resolution scanning mirror and then focused by a 40× objective (N.A. = 0.6) into a diffraction-limited spot (~1 μm) on graphene transistors (Bottom panel of Figure 1A). The photocurrent signals were collected using a preamplifier and the corresponding reflection image was recorded by a silicon detector. By overlapping the reflection image with the photocurrent image, the corresponding position of the photoresponse on the sample could be located.

Figures 2A–2D show the fluorescence, optical, reflection, and photocurrent images of a living retina in a graphene-integrated microfluidic platform, respectively. Pronounced photocurrent responses were observed at graphene-metal junction areas with opposite polarity for drain and source electrodes, because the Schottky-like barriers between metals and graphene can efficiently separate photo-excited EHPs (Detailed photocurrent generation mechanisms will be discussed later). More importantly, remarkable photocurrent signals were detected in the ONH region of the living retinal tissue (Figure 2D), indicating that the electrical activity of the ONH can modulate the carrier concentration of graphene and induce photocurrent signals. The photocurrent responses around the bottom electrode are much weaker than those around the upper electrode, which is likely due to the electrical double layer formed between the retina and graphene that can screen the electrical signals from the retina and reduce the photocurrent responses in graphene. As shown in Figure 2A, the fluorescence image at the region close to the bottom electrode is out-of-focus, suggesting that the ONH did not contact the graphene substrate around the bottom electrode region well. This mainly results from the naturally curved shape of retina, which is not ideally compatible with the planar nature of graphene-integrated microfluidic platforms. If we can fabricate graphene transistors on flexible substrates (such as PDMS membranes), this issue is likely to be addressed. We also investigated electrical signals in the retina after it was dehydrated for 24 hours. During dehydration, the retinal tissue shrunk, slid, and made a good contact with the graphene substrate (Figure 2E and 2F). However, the electrical properties associated with living retina were eradicated. No significant photocurrent response was observed from the entire dehydrated retina, except the graphene-metal junction areas. As shown in Figure 2H, the strong photocurrent signals induced by the living ONH shown in Figure 2D disappeared when the ONH was dehydrated and moved away from its previous location, confirming that the photocurrent responses underneath the living ONH were induced by its electrical activity.

To further validate our result, we studied the electrical signals in a paraformaldehyde-fixed retina through scanning photocurrent measurements. Note that release cuts extending to the ONH in the retina was necessary to relieve the stiffness after fixation and successfully flatten the retina for contact with the graphene (Figure 3A). During the fixation process, the tissue structure was preserved but biochemical reactions were terminated. As we expected, there is no electrical activity in the fixed retina and thus no photocurrent signal was detected in the ONH region (Figure 3B–3D). Comparing the photocurrent results from a living retina with those from dehydrated and fixed retina, we verify that our graphene-based scanning photocurrent microscopy is a promising tool to detect electrical signals in living retina.

For better understanding of the photocurrent generation mechanisms in graphene transistors underneath living retina, relative potential profiles across graphene transistors were extracted by numerical integration of the scanning photocurrent profiles along the dashed lines in Figure 2D and 2H.²⁹ The results in Figure 4A reveal that for the case with dehydrated retina, potential gradients of graphene only exist near the gold electrodes, which are induced by two back-to-back Schottky-like barriers at graphene-metal junction areas. These local electric fields can efficiently separate photo-excited EHPs and lead to strong photocurrent signals at the graphene-metal junction areas as shown in Figure 2H. The polarity of photocurrent responses depends on the direction in which the band bends. For example, with the assistance of the local electric field near the left electrode, photo-induced electrons and holes will travel to the left and right directions, respectively and lead to a current along the right direction. However, excess electrons and holes will travel to opposite directions near the right electrode and generate a photocurrent along the left direction. In addition, a flatband region is formed in the middle of graphene between two electrodes, where the photo-excited EHPs quickly recombine and thus no strong photocurrent response is detected. In contrast, when a living retina is placed on top of a graphene transistor, the cell bodies of RGCs that have neural activity initiated action potentials along their axons can change the local electrochemical environments of the underneath graphene. As a result, the band structure of the graphene will be bent in the areas with neural activities since charged molecules and local potentials can modulate the carrier concentration of graphene and induce local potential gradients (the curved potential between the two electrode in Figure 4B), which can promote separation of photo-excited EHPs and thus photocurrent generation. Different polarities of photocurrent signals are directly related to the bending directions of local potentials. Moreover, the existence of the electrical double layer between graphene and the retina may shield the charged molecules when the layer thickness is beyond the Debye screening length.³⁰ Therefore, only the electrical activity in the regions (such as the ONH), which directly contact or are extremely close to the graphene transistors, can induce strong photocurrent signals in graphene.

CONCLUSIONS

In conclusion, we develop a graphene-integrated microfluidic platform to investigate the electrical activity in mouse retinal tissues through spatially-resolved scanning photocurrent measurements. Remarkable photocurrent signals are detected in the ONH, suggesting that the electrical activity of RGC axons in the ONH can modulate the carrier concentration, induce local potential gradients, and thus produce photocurrent signals in the graphene transistors. Importantly, as control experiments, we find that no significant photocurrent response is observed in graphene underneath both dehydrated and fixed retinal tissues, which further confirms that graphene-based scanning photocurrent microscopy is a promising technique to investigate electrical processes in living retina. This method also opens the door for investigating cellular interactions in other neural networks and biological systems.

METHODS

Graphene synthesis

Copper foils (Alfa Aesar 0.025mm, 99.8% pure, annealed, uncoated) with a grain size of ~100 μm were cut into strips of 1 cm in width and then rinsed with 5% nitric acid (5 min) to eliminate contaminations. We then loaded the copper foils onto a quartz boat, which was transferred to a horizontal furnace system. After the system was pumped down to 10 mTorr, the copper foil was annealed at 980 °C with 100 sccm hydrogen flowing through the tube for 1 hour. A mixed gas of 100 sccm H_2 and 20 sccm CH_4 was then introduced into the furnace for the growth of graphene at 980 °C for 30 minutes.

Device fabrication

The gold electrode arrays were patterned on 170 μm thick coverslips via photolithography, and deposited by e-beam evaporation with 5 nm Ti and 40 nm Au. 6×6 mm squares were then cut from a graphene/copper-foil. After spin-coated by an ultrathin poly(methyl methacrylate) (PMMA) layer, a wet etching process was performed to remove the copper foil. The PMMA/graphene film was then transferred to the coverslip with pre-patterned gold electrodes. To remove PMMA and clean the transistors, acetone (overnight), isopropyl alcohol (10 min), and deionized water baths were used. For microfluidic platforms, a liquid PDMS base polymer was mixed with a curing agent at a 10:1 mass ratio and poured over the wafer in a petri dish, which was degassed in a vacuum chamber for 1 hour and cured at 70 °C for 3 hours. The solid PDMS layer was then cut into a 15×15 mm square with a punched hole in the center and attached to the coverslip with pre-fabricated graphene transistors. A slice of agar gel was placed inside an 8 mm diameter glass cylinder. Once the retina was excised, it was placed and flattened on top of the agar gel. The cylinder was then inverted and placed into the hole of the PDMS layer on the coverslip. Culture media were added into the cylinder to keep the retina healthy.

Animal procurement and ethics statement

This study was conducted in accordance with regulations set forth in the ARVO Statement for the Use of Animals in Ophthalmic and Vision Research. Animal protocols were approved by the Institutional Animal Care and Use Committee of Vanderbilt University Medical Center. B6129SF2/J mice were obtained from Jackson Laboratories (Bar Harbor, ME) and colonies were established in the animal facility at Vanderbilt University Medical Center. Mice utilized in this study were obtained from these in-house colonies.

Neural tracing

Neural tracing was performed as previously described.³¹ Briefly, anesthetized (2.5% isoflurane) adult mice (2 – 4 months) received a 1.5–2 μl intravitreal injection of CTB (10 $\mu\text{g}/\mu\text{l}$ in sterile PBS; Life Technologies) using a 33 gauge needle attached to a Hamilton syringe. Three days after CTB injection, mice were sacrificed by cervical dislocation and decapitation for live or dehydrated retina recordings or by transcardial perfusion with 4% paraformaldehyde for fixed retina recordings.

Organotypic retina culture

Eyes were enucleated and retina was dissected for mounting in the microfluidic platform. Whole retina was maintained for 5 hours in the microfluidic device with serum-free, B27-supplemented medium (NeuroBasal; Gibco, Carlsbad, CA), as previously described.^{32, 33} Media also contained 2 mM glutamine, 0.1 % gentamicin, 1 % N2 supplement (500 µg/mL insulin, 10 mg/mL transferrin, 630 ng/mL progesterone, 1.6 mg/mL putrescine, 520 mg/mL selenite; Gibco), 50 ng/mL brain-derived neurotrophic factor (Invitrogen, Carlsbad, CA), 20 ng/mL ciliary neurotrophic factor (Invitrogen) and 100 µM inosine (Sigma, St. Louis, MO).

Acknowledgments

The authors would like to thank Franklin Echevarria for technical assistance. This work was supported by National Institutes of Health (1R21EY026176 and 1R21NS095323) and National Science Foundation (ECCS-1055852, CBET-1264982, and BIO-1450897). The devices were fabricated at the Center for Nanophase Materials Sciences at the Oak Ridge National Laboratory.

References

1. Abrey LE, Batchelor TT, Ferreri AJ, Gospodarowicz M, Pulczynski EJ, Zucca E, Smith JR, Korfel A, Soussain C, DeAngelis LM. *Journal of clinical oncology*. 2005; 23:5034–5043. [PubMed: 15955902]
2. Iseri PK, Altinas Ö, Tokay T, Yüksel N. *Journal of neuro-ophthalmology*. 2006; 26:18–24. [PubMed: 16518161]
3. Imamura Y, Fujiwara T, Margolis R, Spaide RF. *Retina*. 2009; 29:1469–1473. [PubMed: 19898183]
4. London A, Benhar I, Schwartz M. *Nature Reviews Neurology*. 2013; 9:44–53. [PubMed: 23165340]
5. Wang YV, Weick M, Demb JB. *J Neurosci*. 2011; 31:7670–7681. [PubMed: 21613480]
6. Arman AC, Sampath AP. *J Vis Exp*. 2010; 43:2107.
7. Sucher NJ, Aizenman E, Lipton SA. *The Journal of neuroscience*. 1991; 11:966–971. [PubMed: 1672708]
8. Kitamura K, Judkewitz B, Kano M, Denk W, Häusser M. *Nature methods*. 2008; 5:61–67. [PubMed: 18157136]
9. Kim SA, Jun SB. *Exp Neurobiol*. 2013; 22:158–166. [PubMed: 24167411]
10. Denk W, Detwiler PB. *Proceedings of the National Academy of Sciences*. 1999; 96:7035–7040.
11. Scanziani M, Häusser M. *Nature*. 2009; 461:930–939. [PubMed: 19829373]
12. Obien ME, Deligkaris K, Bullmann T, Bakkum DJ, Frey U. *Front Neurosci*. 2014; 8:423. [PubMed: 25610364]
13. Hughes S, Rodgers J, Hickey D, Foster RG, Peirson SN, Hankins MW. *Sci Rep*. 2016; 6:28086. [PubMed: 27301998]
14. Bertotti G, Dodel N, Keil S, Wolansky D, Tillak B, Schreiter M, Eickenscheidt M, Zeck G, Stett A, Möller A. A capacitively-coupled CMOS-MEA with 4225 recording sites and 1024 stimulation sites. 2014
15. Lee S, Jung SW, Ahn J, Yoo HJ, Oh SJ. *Journal of Micromechanics and Microengineering*. 2014; 24:075018.
16. Spira ME, Hai A. *Nat Nanotechnol*. 2013; 8:83–94. [PubMed: 23380931]
17. Novoselov KS, Geim AK, Morozov S, Jiang D, Zhang Y, Dubonos Sa, Grigorieva I, Firsov A. *science*. 2004; 306:666–669. [PubMed: 15499015]
18. Neto AC, Guinea F, Peres N, Novoselov KS, Geim AK. *Rev Mod Phys*. 2009; 81:109.
19. Mueller T, Xia F, Avouris P. *Nat Photonics*. 2010; 4:297–301.
20. Engel M, Steiner M, Lombardo A, Ferrari AC, Löhneysen Hv, Avouris P, Krupke R. *Nat Commun*. 2012; 3:906. [PubMed: 22713748]
21. Wang Y, Shao Y, Matson DW, Li J, Lin Y. *Acs Nano*. 2010; 4:1790–1798. [PubMed: 20373745]

22. Fan H, Wang L, Zhao K, Li N, Shi Z, Ge Z, Jin Z. *Biomacromolecules*. 2010; 11:2345–2351. [PubMed: 20687549]
23. Pinto AM, Gonçalves IC, Magalhães FD. *Colloids and Surfaces B: Biointerfaces*. 2013; 111:188–202. [PubMed: 23810824]
24. Liu S, Guo X. *NPG Asia Materials*. 2012; 4:e23.
25. Dodson KH, Echevarria FD, Li D, Sappington RM, Edd JF. *Biomedical microdevices*. 2015; 17:1–10. [PubMed: 25653054]
26. Li X, Cai W, An J, Kim S, Nah J, Yang D, Piner R, Velamakanni A, Jung I, Tutuc E. *Science*. 2009; 324:1312–1314. [PubMed: 19423775]
27. Abrahamson EE, Moore RY. *Brain research*. 2001; 916:172–191. [PubMed: 11597605]
28. Govardovskii VI, FYHRQUIST N, Reuter T, KUZMIN DG, DONNER K. *Visual neuroscience*. 2000; 17:509–528. [PubMed: 11016572]
29. Mueller T, Xia F, Freitag M, Tsang J, Avouris P. *Phys Rev B*. 2009; 79:245430.
30. Largeot C, Portet C, Chmiola J, Taberna PL, Gogotsi Y, Simon P. *Journal of the American Chemical Society*. 2008; 130:2730–2731. [PubMed: 18257568]
31. Formichella CR, Abella SK, Sims SM, Cathcart HM, Sappington RM. *Journal of clinical & cellular immunology*. 2014; 5:188. [PubMed: 25133067]
32. Sappington RM, Chan M, Calkins DJ. *Investigative ophthalmology & visual science*. 2006; 47:2932–2942. [PubMed: 16799036]
33. Sappington RM, Sidorova T, Long DJ, Calkins DJ. *Investigative ophthalmology & visual science*. 2009; 50:717–728. [PubMed: 18952924]

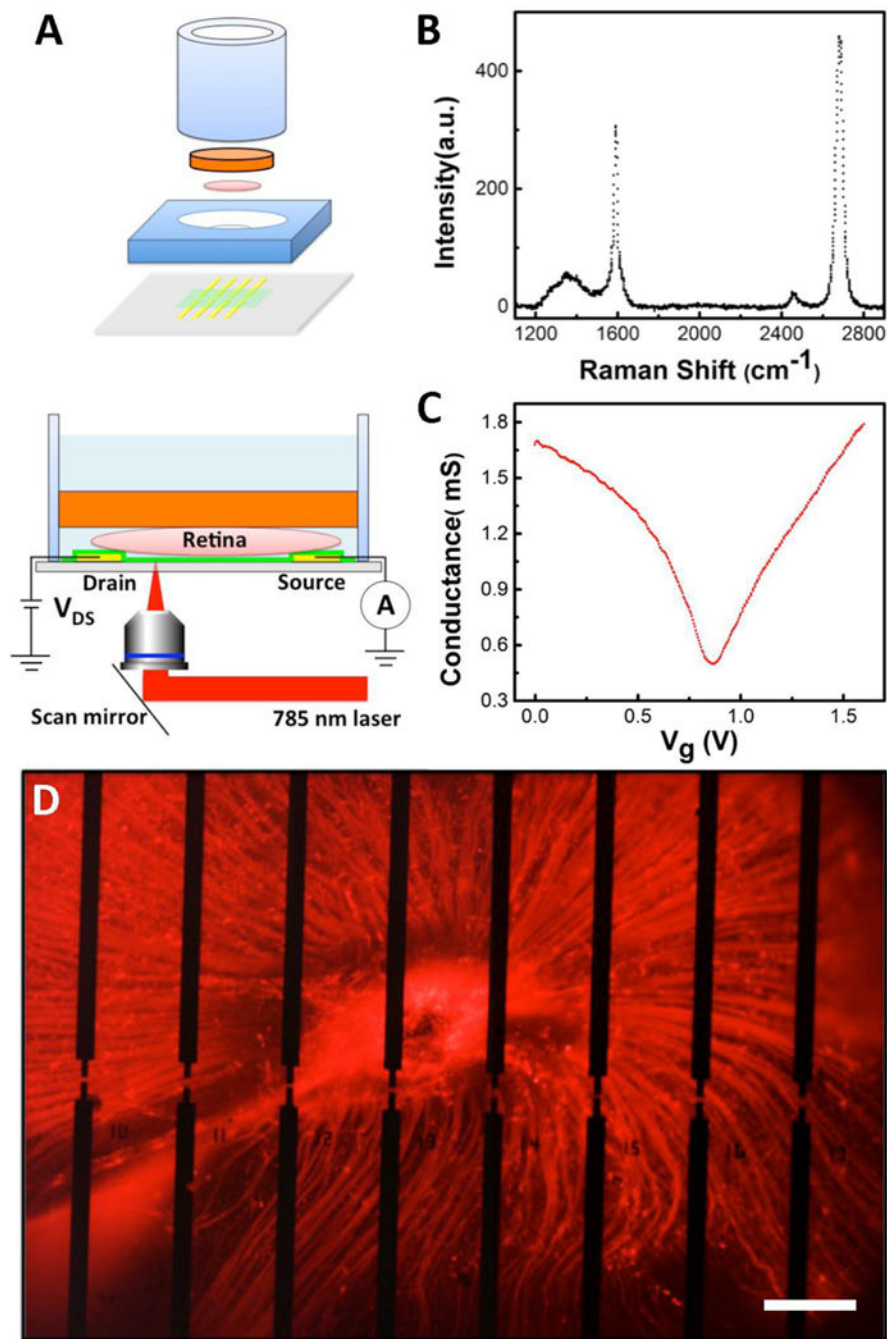


Figure 1. Overview of the experimental design. (A) Top: Exploded view of a graphene-integrated microfluidic platform. The orange plate is a slice of agar gel. The pink disk represents a retina. The green plane indicates a graphene film. The yellow bars represent Au electrodes. Bottom: Schematic diagram of scanning photocurrent measurements. A one micron diameter diffraction-limited laser spot goes through a transparent coverslip to scan over graphene transistors underneath a retinal tissue in a microfluidic platform. (B) Raman spectrum of graphene on a coverslip. (C) Electrolyte gate response of a typical graphene transistor. (D)

Fluorescence image of a CTB-labeled retina on top of graphene transistors. There are 54 separated electrodes in an electrode array, where the edge-to-edge distances between two electrodes in the horizontal direction is 180 μm and between upper and lower electrodes are 20 μm , 40 μm , and 60 μm , respectively. A graphene film is placed on top of all electrodes. Any two electrodes can be used as source and drain electrodes, respectively. Here, 16 opaque electrodes near the ONH are imaged. Scale bar is 200 μm .

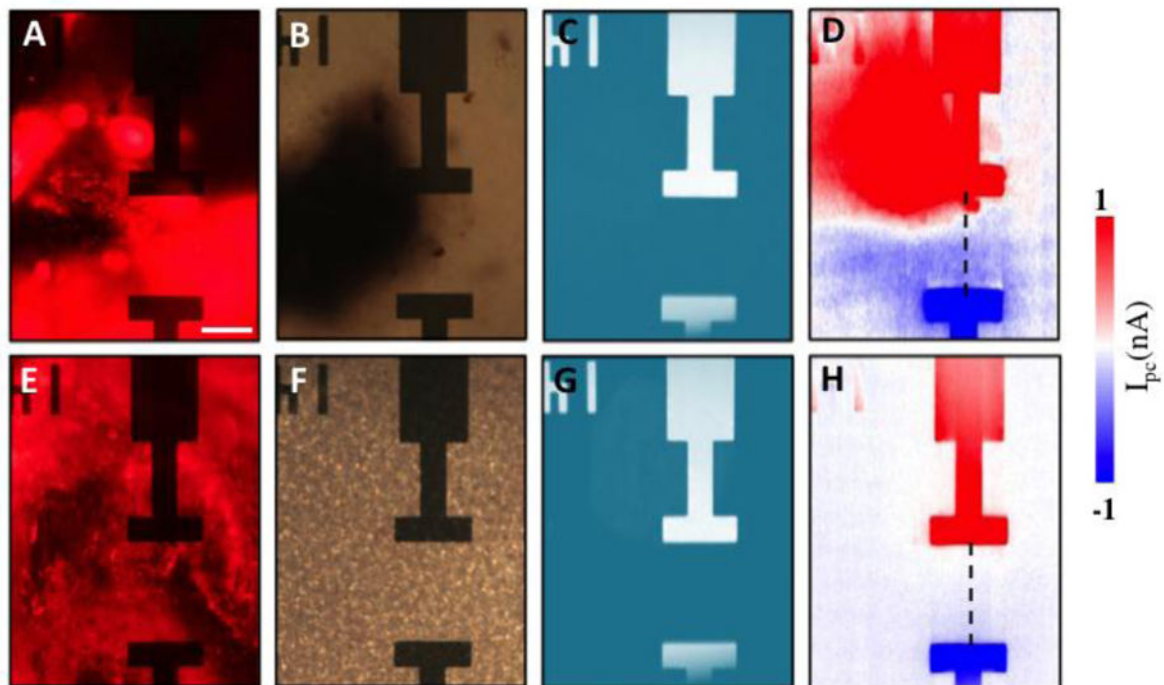


Figure 2.

(A) Fluorescence, (B) optical, (C) reflection and (D) scanning photocurrent images of a fresh excised, CTB-labeled retina on top of a graphene transistor in the ONH region, respectively. (E) Fluorescence, (F) optical, (G) reflection and (H) scanning photocurrent images of the retina/graphene at the same location after it is dehydrated at room temperature for 24 hours, respectively. Source and drain electrodes are $45\ \mu\text{m}$ by $15\ \mu\text{m}$. The edge-to-edge distance between two electrodes is $60\ \mu\text{m}$. Scale bar is $30\ \mu\text{m}$. The inverted '14' near the upper electrode is a metal marker for location.

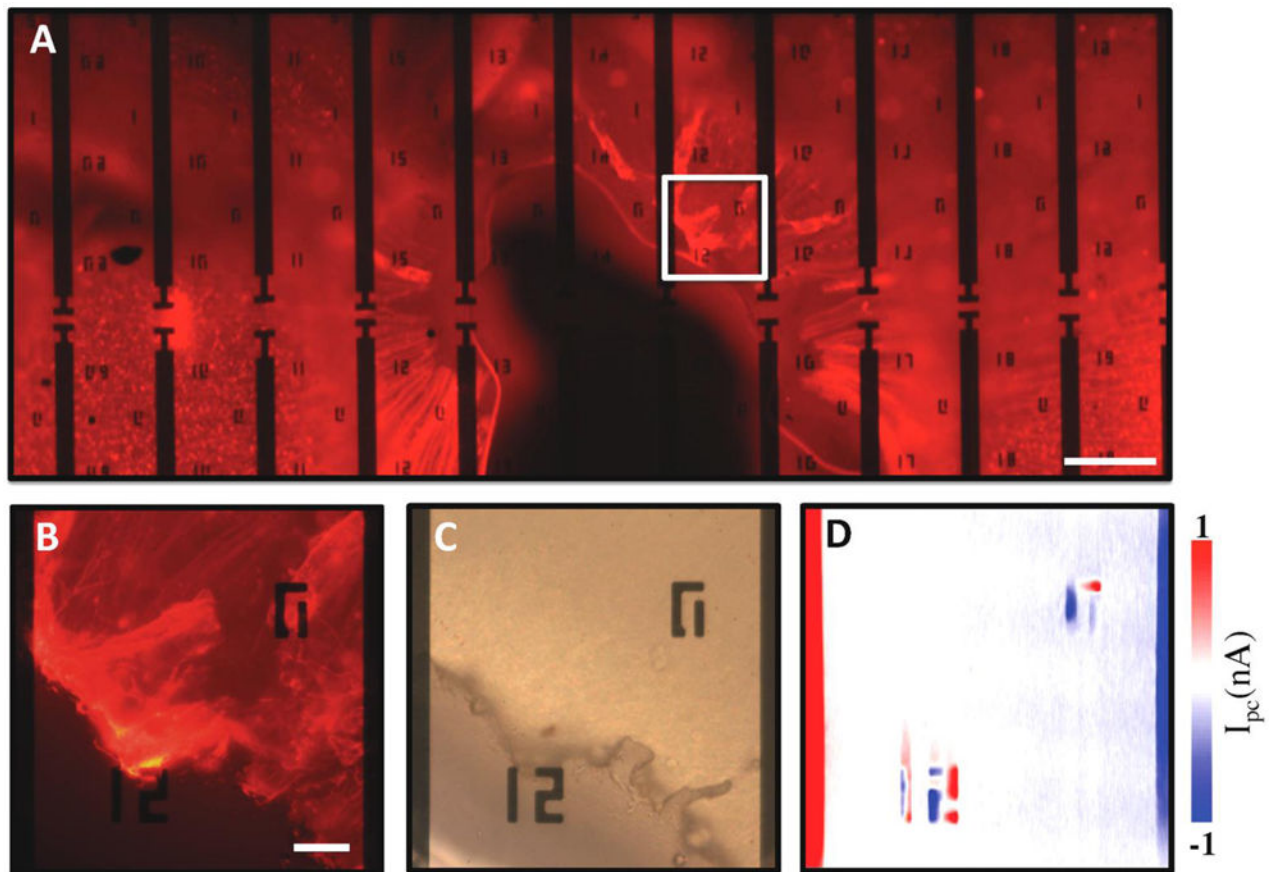


Figure 3.

(A) Fluorescence image of a fixed retina. Scale bar is 200 μm . (B) Enlarged fluorescence, (C) optical, and (D) scanning photocurrent images of the retina in the ONH region, respectively. The edge-to-edge distance between two electrodes is 180 μm . Scale bar is 30 μm in B–D. ‘12’ and ‘0’ near electrodes are metal markers for location.

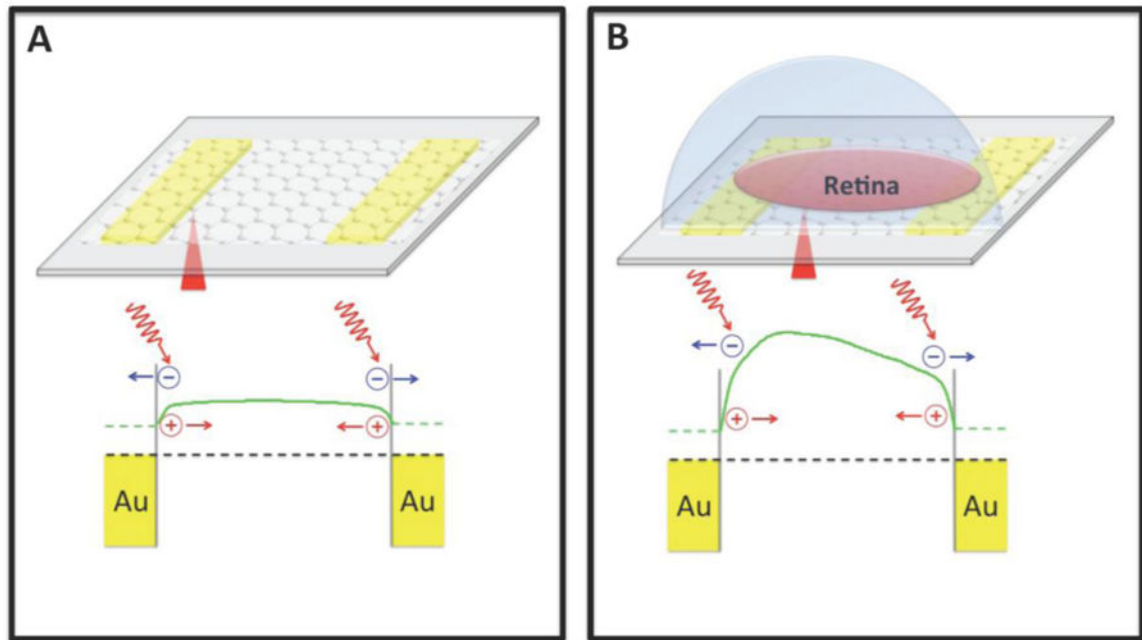


Figure 4. Schematic diagrams of band structures of a graphene transistor. (A) Photocurrent signals generate at graphene-metal junction areas due to the band structure bending. (B) A retina can modulate the carrier concentration of graphene underneath it. Green solid lines show potential profiles. Black dashed lines denote the Fermi levels. Note that in (A) and (B), the potential profiles are obtained through numerical integration of the scanning photocurrent profiles along the dashed lines in Figure 2H and 2D, respectively.